УДК 531.011

M.B. Liu, G.R. Liu
(National University of Singapore),
K.Y. Lam, Z. Zong
(Institute of High Performance Computing, Singapūre)

Comparative Study of the Real and Artificial Detonation Models in Underwater Explosion Simulations

This paper presents a comparative investigation on the real and artificial detonation models as well as their influences to the entire underwater explosion simulations. The study is carried out by using the meshless, Lagrangian, and particle method—smoothed particle hydrodynamics, which is robust, easy to apply and computationally efficient. Numerical results show that the real detonation model produces more reasonable results than the artificial detonation model.

Представлен сравнительный анализ моделей реальной и искусственной детонации и их влияния на моделирование подводных взрывов. Для решения поставленной задачи использован численный гидродинамический метод сглаженных частиц, который является не сеточным и основан на свойствах частиц Лагранжа. Этот метод устойчив, прост в реализации и вычислительно эффективен. Показано, что модель реальной детонации дает лучшие результаты, чем модель искусственной детонации.

K e y w o r d s: detonation model, underwater explosion, detonation wave propagation.

Underwater explosion involves in violent chemical reaction which converts the original high explosive (HE) into gas at very high temperature and pressure, occurring with extreme rapidity and evolving a great deal of heat. Simulation of underwater explosion problems is a big challenge for traditional numerical methods. Early theoretical and numerical analyses of underwater explosions were generally based on the assumptions that the explosive charge in the spherical shape detonated from the charge center and the surrounding water was infinite [1—3]. In the numerical implementations, the pressure in the explosive gas was determined empirically, while the interaction between the explosive gas and the surrounding water was not properly considered. These disadvantages generally restricts the prediction of the peak pressure to be acceptable beyond the range of more than 10 times the spherical charge radius.

Many early numerical analyses of underwater explosions employed an artificial detonation model of adiabatic explosion at constant volume rather than the real

detonation process of HE in the entire underwater explosion simulations. In this artificial detonation model, the detonation process of the HE is neglected with assumptions that the detonation velocity is infinite, and the original HE is replaced by or in a sudden converted to a gas globe of extremely high pressure and temperature. The gas globe possesses the same energy, occupies the same space as the original HE, interacts with the surrounding water, and then produces shock waves as well as bubble pulses in the water. Due to the assumptions or simplifications on the real detonation process, this artificial detonation model does not give the proper pressure profiles in the detonation produced gas product. In some later numerical simulations [4, 5], the real detonation process of the HE is included into the entire underwater explosion simulations, and thus the pressure profiles in the explosive gas can be numerically but not empirically determined. These two models on the detonation process of HE yield different physics in the explosive gas and may lead to different results in underwater explosion simulations. However, no comparative investigation has ever been carried out on these two detonation models and their influences to the entire underwater explosion simulations.

In this paper the real and artificial detonation models as well as their influences to the entire underwater explosion simulations are comparatively investigated by using the method of smoothed particle hydrodynamics (SPH). SPH is unique in computational fluid mechanics due to its meshless, Lagrangian and particle features. Since its invention to solve astrophysical problems in three-dimensional open space [6—8], SPH has been heavily studied and extended to dynamic response with material strength [9—11] as well as dynamic fluid flows with large distortions [12]. SPH uses smoothed particles as interpolation points to represent materials at discrete locations, so it can easily trace material interfaces, free surfaces and moving boundaries. The meshless nature of SPH overcomes the difficulties due to large deformations since SPH uses particles or points rather than mesh as computational frame to interpolate. These nice features of SPH make it fairly attractive in simulating underwater explosion. Numerical analyses are carried out for TNT explosion in water with one case of slab charge and another case of spherical charge. The different performances of these two detonation models on the shock wave propagation and peak shock pressure will be investigated.

Underwater explosion simulation. The underwater explosion can be divided into two processes, the detonation process through the HE and the dispersion process of the detonation-produced gas, which interacts with the surrounding water. In underwater explosions, the explosive gas and the water can be assumed to be inviscid and compressible while the explosion process adiabatic. So the Euler equa-

tion can be used to model the explosive gas as well as the water coupled with corresponding equation of state

$$\begin{aligned} \frac{D\rho}{Dt} &= -\rho\nabla\mathbf{v}, \\ \frac{D\mathbf{v}}{Dt} &= -\frac{1}{\rho}\nabla p, \\ \frac{Du}{Dt} &= -\frac{p}{\rho}\nabla\mathbf{v}, \\ p &= p(\rho,u), \end{aligned} \tag{1}$$

where $\mathbf{v}$, u, ρ, p and t are velocity vector, internal energy, density, pressure and time instant respectively. The first three equations in equation (1) state the conservation of mass, momentum and energy, while the fourth equation is the equation of state (EOS). In this paper TNT is used in the simulation as the HE and the detonation gas product is assumed to behave as a Jones-Wilkins-Lee (JWL) high energy explosive with the equation of state

$$p = A\left(1-\frac{\omega\theta}{R_1}\right)e^{-\frac{R_1}{\theta}} + B\left(1-\frac{\omega\theta}{R_2}\right)e^{-\frac{R_2}{\theta}} + \omega\theta\rho_0 E, \tag{2}$$

where the parameters are $A = 3.712\times10^{11}$ Pa; $B = 0.0321\times10^{11}$ Pa; $R_1 = 4.15$; $R_2 = 0.95$; $\omega = 0.30$; $\theta = \rho/\rho_0$; ρ_0 is the reference density of 1630 kg/m^3; E is the initial specific internal energy of 4.29×10^6/kg. The detonation velocity of 6930 m/s is used.

The equation of state for water is

$$p = a_1\mu + a_2\mu^2 + a_3\mu^3 + (b_0 + b_1\mu)\rho u,$$

where $\mu = \rho_w/\rho_0 - 1$; $a_1 = 2.2\times10^9$ N/m^2; $a_2 = 9.54\times10^9$ N/m^2; $a_3 = 1.457\times10^{10}$ N/m^2; $b_0 = 0.28$; $b_1 = 0.28$; $\rho_0 = 1000$ kg/m^3.

Numerical method-SPH methodology. As a Lagrangian particle method, the basic concept of SPH is that the state of a system can be determined by a collection of arbitrarily distributed particles while forces are calculated through inter-particle interactions in a smoothed fashion. These smoothed particles can be regarded as interpolation points, which form the computational frame for the differential equations given in equation (1). The particle properties can be estimated by taking a weighted average value over those of the surrounding particles.

Numerical approximation. In SPH methodology, the fluid is represented by particles, which are typically of fixed mass, follow the fluid motion, advect contact discontinuities and reduce computational diffusion of various fluid properties. The particles carry fluid quantities such as mass m, velocity vector $\mathbf{v}$, position vector $\boldsymbol{x}$ etc, and form the computational frame for the partial differential equations governing the conservation law. In the standard SPH methodology, for a function f, the approximation of its function value at a certain location or particle i as well as its gradient can be expressed as summation interpolants over the neighbor particles using a smoothing kernel function W with the smoothing length h

$$\langle f_i \rangle = \sum_{j=1}^{N} \left(\frac{m_j}{\rho_j} \right) f_j W_{ij} ,$$

$$\langle \nabla f_i \rangle = \sum_{j=1}^{N} \left(\frac{m_j}{\rho_j} \right) f_j \nabla_i W_{ij} ,$$

where if representing the distance between particle i and j as r_{ij},

$$W_{ij} = W(\boldsymbol{x}_i - \boldsymbol{x}_j, h) = W(|\boldsymbol{x}_i - \boldsymbol{x}_j|, h),$$

$$\nabla_i W_{ij} = \frac{\boldsymbol{x}_i - \boldsymbol{x}_j}{r_{ij}} \frac{\partial W_{ij}}{\partial r_{ij}} = \frac{\boldsymbol{x}_{ij}}{r_{ij}} \frac{\partial W_{ij}}{\partial r_{ij}}$$

where $\boldsymbol{x}$ is the position vectors of the particles.

A typical smoothing kernel function should satisfy the requirements of normalization condition, $\int W(\boldsymbol{x} - \boldsymbol{x}', h)\, d\boldsymbol{x} = 1$; Delta function condition, $\lim_{h \to 0} W(\boldsymbol{x} - \boldsymbol{x}', h) = \delta(\boldsymbol{x} - \boldsymbol{x}')$ as $h \to 0$; and the compactness condition, $W(\boldsymbol{x} - \boldsymbol{x}', h) = 0$ for $|\boldsymbol{x} - \boldsymbol{x}'| > \lambda h$, where λ is a constant dependent only on the particular smoothing kernel function used. In this paper, the cubic spline function is used [8],

$$W(S, h) = \alpha_d \begin{cases} \frac{2}{3} - S^2 + \frac{1}{2} S^3, & 0 \le S < 1, \\ \frac{1}{6}(2 - S)^3, & 1 \le S < 2, \\ 0, & S \ge 2, \end{cases}$$

where $S = |\boldsymbol{x} - \boldsymbol{x}'| / h$; α_d is a dimension-dependent constant related to the smoothing length. In one, two or three-dimensional space $\alpha_d = 1/h$, $15/7\pi h^2$ or $3/2\pi h^3$ respectively. It's clear that the λ used in this cubic spline kernel is 2.

Artificial viscosity. The artificial viscosity is used in SPH methodology to stabilize the numerical scheme, prevent particle penetration and capture shock waves. In this paper, we employ the standard Monaghan type artificial viscosity Π_{ij} [8],

$$\Pi_{ij} = \begin{cases} \dfrac{-\alpha \bar{c}_{ij}\mu_{ij} + \beta\mu_{ij}^2}{\bar{\rho}_{ij}}, \mathbf{v}_{ij}\cdot\boldsymbol{x}_{ij} < 0, \\ 0, \mathbf{v}_{ij}\cdot\boldsymbol{x}_{ij} \geq 0, \end{cases}$$

$$\mu_{ij} = \frac{h_{ij}\mathbf{v}_{ij}\cdot\boldsymbol{x}_{ij}}{|r_{ij}|^2 + \eta^2}, \quad \bar{c}_{ij} = \frac{1}{2}(c_i + c_j), \quad \bar{\rho}_{ij} = \frac{1}{2}(\rho_i + \rho_j),$$

$$\mathbf{v}_{ij} = \mathbf{v}_i - \mathbf{v}_j, \quad h_{ij} = \frac{1}{2}(h_i + h_j),$$

where α,β,η are constants that are set 1, 10 and $0.1h_{ij}$; $\mathbf{v}$ and c represent the velocity vector and the speed of sound respectively.

Equation of motion. Applying the SPH kernel and particle approximation concept to equation (1), the following discretized equation of motion is derived as one of the standard form of SPH equations and can be used to model the HE detonation as well as the underwater explosions

$$\frac{D\rho_i}{Dt} = \sum_{j=1}^{N} m_j(\mathbf{v}_i - \mathbf{v}_j)\nabla_i W_{ij},$$

$$\frac{D\mathbf{v}_i}{Dt} = -\sum_{j=1}^{N} m_j \left(\frac{p_i}{\rho_i^2} + \frac{p_j}{\rho_j^2} + \Pi_{ij} \right) \nabla$$

$$\frac{Du_i}{Dt} = \frac{1}{2}\sum_{j=1}^{N} m_j \left(\frac{p_i}{\rho_i^2} + \frac{p_j}{\rho_j^2} + \Pi_{ij} \right) (\mathbf{v}_i - \mathbf{v}_j)\nabla_i W_{ij},$$

$$\frac{Dx_i}{Dt} = \mathbf{v}_i$$

Using some standard techniques such as leapfrog (LF), predictor-corrector and Runge-Kutta (RK) schemes can carry out the numerical integration of ordinary differential equation for physical variables at every particle. In this paper, the leapfrog

method is used for its low memory storage and efficiency. The particle density, velocity, internal energy and position can be updated in the following formulations:

$$
\begin{aligned}
t &= t + \Delta t, \\
\rho_i(t + \Delta t/2) &= \rho_i(t - \Delta t/2) + \Delta t \cdot D\rho_i(t), \\
\mathbf{v}_i(t + \Delta t/2) &= \mathbf{v}_i(t - \Delta t/2) + \Delta t \cdot D\mathbf{v}_i(t), \\
u_i(t + \Delta t/2) &= u_i(t - \Delta t/2) + \Delta t \cdot Du_i(t), \\
\boldsymbol{x}_i(t + \Delta t) &= \boldsymbol{x}_i(t) + \Delta t \cdot \mathbf{v}_i(t + \Delta t/2).
\end{aligned}
$$

However, the LF is subject to the CFL condition for stability, which typically results in time step to be proportional to the smoothing lengths. In this work, the time step is taken as

$$\Delta t = \min\left(\xi h_i / [h_i(\nabla \mathbf{v}_i + c_i + 1.2\,(\alpha c_i + \beta |\nabla \mathbf{v}_i|)]\right),$$

where ξ is the Courant number, taken around 0.3.

Numerical tests and analyses. ***HE detonation process.*** The difference and concern of the two detonation models lie in whether the real detonation process has been included into the entire underwater explosion simulations or the real detonation process is simplified as an artificial detonation condition of adiabatic explosion at constant volume. In this work, the real detonation process of a one dimensional TNT slab is first investigated to study the distribution of the physical variables in the gas which will affect the later shock wave. This case is specially selected for the purpose of comparison since good numerical simulations [5, 13] for the same case have already been given. The simulation of one-dimensional TNT slab detonation doesn't lose generality since early analyses based on the assumption of spherical charge detonating from the charge center can be simplified into one dimension.

In the simulation, a 0.1 m long TNT slab is detonated from one end. In Shin's simulation, coupled Lagrangian-Eulerian analysis with the software MSC/Dytran is applied. The wall boundary conditions were used to forbid material transport from everywhere. In this SPH simulation, the symmetric condition is used. This makes the detonation of the 0.1 m long slab from one end to the other end equivalent to the detonation of a 0.2 m long slab from the middle point to one end. Before detonation, particles are evenly distributed along the slab. The initial smoothing length is one and a half times the particle separation. After detonation, a plane detonation wave is produced. According to the detonation velocity, it takes around 14.4 μs to complete the detonation to the end of the slab.

Figures 1, 2, 3 show the pressure, density and velocity along the slab at 1 μs interval from 1 to 14 μs by using 4000 particles. The dashed line in Fig. 1 represents

the experimentally determined C-J detonation pressure, which is, according to the Chapman and Jouguet's hypothesis, the pressure at the tangential point of the Hugoniot curve and the Rayleigh line [4, 14] and represents the pressure at the equilibrium plane at the trailing edge of the very thin chemical reaction zone. For this one-dimensional TNT slab detonation problem, the C-J pressure is 2.1×10^{10}N/m^2. It can be seen from Fig. 1 that the gas behind the detonation wave front has a pressure profile similar to a step increase followed by exponential type decay, with the peak pressure immediately behind the detonation wave front and the decay length increasing with propagation distance. With the process of the detonation, the detonation pressure converges to the C-J pressure. The detonation shock is resolved within several smoothing lengths. Further investigation reveals that more particles along the slab result in sharper pressure profiles with bigger peak pressures. The results are quite accurate and comparable to the results obtained by Shin.

For the simplified artificial detonation, the high explosive is replaced by explosive gas in a sudden, which occupies the same volume with the same energy, so the density also remains the same, as shown by the dotted line on Fig. 2. It's different from the above calculated density profile, which behaves as a step increase followed by an exponential type decay. The gas particles are not in motion at this instant and so the particle velocity is zero. The pressure of the gas calculated by using equation (2) with $\rho/\rho_0 = 1$ is around 8.3759e + 009 N/m^2 and is shown by the dotted line on Fig. 1, this value is between the above calculated forward peak pressure and the backward steady pressure, much smaller than peak pressure, while bigger than the steady pressure. Since the detonation process is neglected in this artificial detonation model, no detonation shock will advance along the TNT slab, while the pressure suddenly rises to a very high level with its front at the gas/water interface.

Besides the different distribution of the physical variables, the real detonation also causes two shaded areas both in Figures 1 and 2 at different instants. The shaded areas in Figures 1 and 2 are for the instants of 14 μs. It is found that the upper shaded area is approximately equal to the lower shaded area in the density profile in Fig. 2, which is a reflection of the mass conservation in these two models. For pressure distribution in Fig.1, the upper shaded area is bigger than the lower shaded area. This suggests when considering the detonation process, the gas will exert bigger force on the surrounding water after the detonation is finished. It's reasonable to presume that the differences of the distribution of the physical variables in the high explosive gas will lead to different performances when interacting with the surrounding water, and may lead to different shock behavior in the water.

TNT slab explosion in water. After detonation of the high explosive, the explosive gas of high pressure, temperature and velocity tends to move outside, and interacts with the surrounding water. For the above case, the interacting dispersion pro-

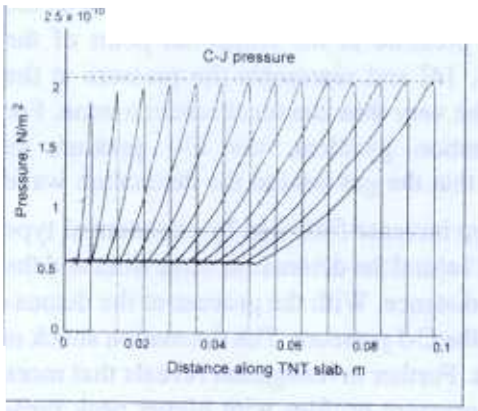

Fig. 1. Pressure profiles along the TNT slab

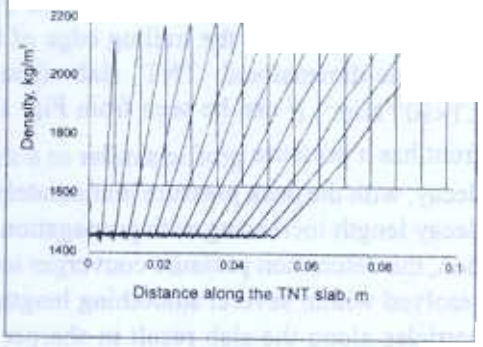

Fig. 2. Density profiles along the TNT slab

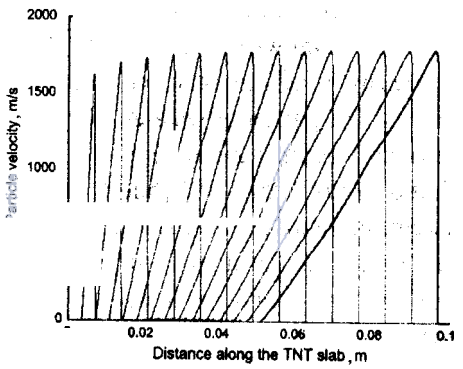

Fig. 3. Velocity profiles along the TNT slab

cess of the explosive gas to outside water is investigated here. In the simulation the computational domain of water is 10 m, which is large enough to prevent the boundary effect.

Figure 4 shows the peak shock pressure in the water at different locations. In the figure, a is the length of the original HE charge length, R is the distance from the pressure measure location to the detonation end of the charge. It can be seen that the peak pressures in both models decrease as the shock waves move away from the explosive gas. The decrease of the peak pressures behaves as an exponential decay. At locations nearer to the charge or explosive gas, the peak pressure for the real detonation model is much bigger than that for the artificial model. As the shock waves advance ahead, the difference becomes smaller. Beyond the range of 8-10 times the charge length, the difference is too small to be negligible.

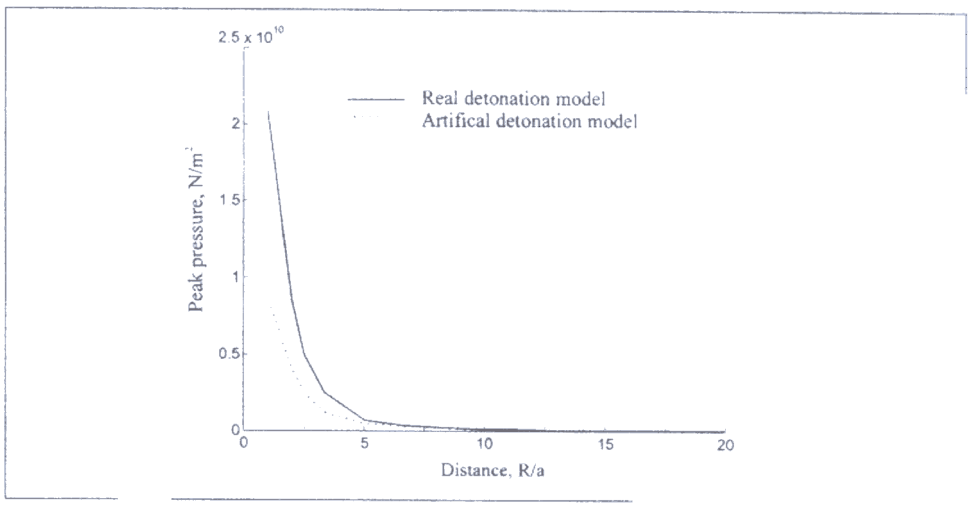

Fig. 4. Peak pressures at different locations for the case of slab TNT charge

Figure 5 shows the pressure history for the location at 0.25 m, which is 2.5 times the length of the original TNT charge. It is obvious that the peak pressure as well as the pressure curve for the real detonation model is higher than that for the artificial detonation model. It is noted that the arrival time for the shock wave to reach the location in the real detonation model is slightly earlier than that in the artificial detonation model. This is another representation of the bigger impulse of the explosive gas to surrounding water in the real detonation model.

Underwater explosion of spherical TNT charge. To further validate our observation that the influence of the two detonation models on the entire underwater explosions only and greatly differs at earlier stages or nearer locations, and is negligible at very far away locations, another numerical test which involves in a spherical TNT of 137 kg is simulated. For the spherical charge detonation from the charge center, some empirical formulae exist to predict the peak shock pressure at different locations [1—3]. One approach is the Penney-Dusgupta theory, which numerically integrate the Riemann equations outward from the charge. According to Penney-Dusgupta theory, for TNT, the value of the peak pressure is as a function of shock radius R and the charge weight W,

$$p_m = 2.86 \cdot 10^7 \left(W^{1/3}/R \right) e^{0.108 W^{1/3}/R}$$

Figure 6 shows the detailed comparisons of peak pressures obtained from different resources, experimental data from [14], the Penney-Dusgupta theoretical

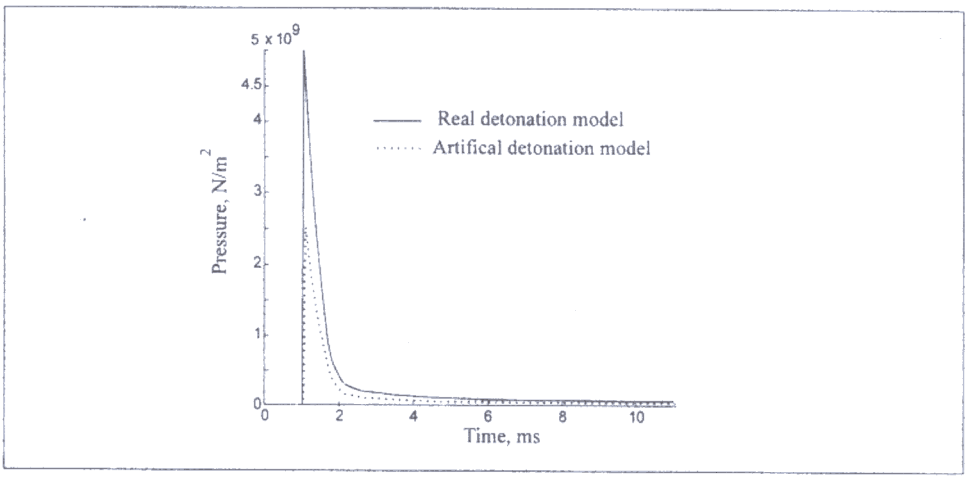

Fig. 5. Pressure history for the location of R/a=2.5 for the case of slab TNT charge

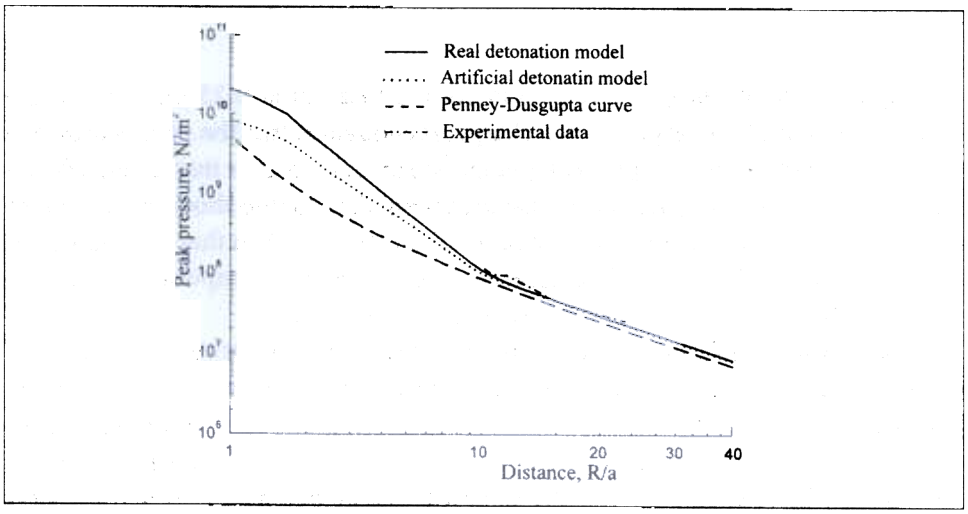

Fig. 6. Peak pressures at different locations for the case of spherical TNT charge

value, and the SPH simulation results with two detonation models. In the logarithm scaled figure, a is the radius of the original HE charge length; R is the distance from the pressure measure location to the charge center. For the region of R/a>10, the Penney-Dusgupta curve can be approximated as a straight line, and compare well with the experimental data. The peak pressure becomes higher for closer distances. It should be noted that the Penney-Dusgupta curve is only valid for the region of R/a > >10; for the region of 10> R/a >1, since the experimental data is not available, the validity of the Penney-Dusgupta theory needs to be further verified. In the SPH sim-

ulation, the peak pressure measure locations in water can be taken from the gas/water interface (R/a=1) to further distances. The numerical results from SPH simulation also agree well with the experimental data and the Penney-Dusgupta curve for the region R/a>10. The peak pressure curves from the two detonation models are both above the Penney-Dusgupta curve, and are closer to the experimental data than the Penney-Dusgupta curve. Similar to the above case of TNT slab explosion in water, the peak pressures in both models decrease as the shock waves propagate ahead. At locations nearer to the charge or explosive gas, the peak pressure for the real detonation model is much bigger than that for the artificial model. Beyond the range of 8-10 times the charge radius, the difference is too small to be negligible.

Conclusions. In this paper the real and the artificial detonation models of HE as well as their influences to the entire underwater explosion simulations are comparatively investigated by using the meshless, Lagrangian method of SPH. The smoothed particle hydrodynamics is robust, easy to apply, computationally efficient and can give good predictions for both magnitude and form of the shock wave. The study is carried out with numerical examples of slab and spherical TNT charge. It is found that the two different detonation models leads to different profiles of physical variables along the high explosive gas, and yields different impulses to the surrounding water. The real detonation model produces stronger impulse than the artificial detonation model. Since the real detonation model properly gives the profiles of physical variables in explosive gas before interacting with water, it leads to more reasonable results. For the artificial detonation model, neglecting the detonation process and simply replacing the original HE charge with explosive gas yield lower peak pressure and slightly later arrival shock wave time. The difference in peak pressure is rather large at closer distances, and become smaller with the advance of the shock wave, and finally turns to be negligible after the region of 8-10 times the charge radius (or equivalently charge length). So it can be concluded that for numerical simulations of underwater explosions, beyond the region of 8-10 times the charge radius, both two detonation models can get fairly good and close results; in region nearer than 8-10 times the charge radius, the real detonation model rather than the artificial detonation model should be employed to obtain more reasonable results.

Подано порівняльний аналіз моделей реальної та штучної детонації та їхній вплив на моделювання підводних вибухів. Для розв'язання поставленої задачі використано чисельний гідродинамічний метод згладжених частинок, який не є сітковим і базується на властивостях частинок Лагранжа. Цей метод є стійким, простим у реалізації та чисельно ефективним. Показано, що модель реальной детонації дає кращі результати, ніж модель штучної детонації.

1. *Kirkwood J.G., Bethe H.A.* Basic propagation theory. — OSRD 558, 1942.
2. *Penney and Dasgupta H.K.* British Report, RC 333, 1942.
3. *Brinkley S.R., Kirkwood J.G.* Theory of the propagation of shock waves // Physics Review, 1947. — **71.** — P. 606.
4. *Charles L. Mader* Numerical Modeling of Detonations. — University of California Press, 1979.
5. *Shin Y.S., Chisum J.E.* Modeling and simulation of underwater shock problems using a coupled Lagrangian-Eulerian analysis approach//Shock and Vibration. — 1997. — **4.** — P. 1—10.
6. *Lucy L.* A numerical approach to testing the fission hypothesis, Astronomical J. — 1977. — **82.** — P. 1013—1024.
7. *Gingold R.A., Monaghan J.J.* Smoothed particle hydrodynamics: theory and application to non-spherical stars // Monthly Notice of the Royal Astronomical Society. — 1977. — **181.** — P. 375—389.
8. *Monaghan J.J.* Smoothed particle hydrodynamics, Annual Review of Astronomical and Astrophysics. — 1992. — **30.** — P. 543—574.
9. *Liberskty L. D., Petsheck A. G., et al.* High strain Lagrangian hydrodynamics-a three-dimensional SPH code for dynamic material response// J. Of Computational Physics. — 1993. — **109.** — P. 67—75.
10. *Randles P. W., Libersky L. D.* Smoothed particle hydrodynamics: some recent improvements and applications // Computer methods in applied mechanics and engineering. — 1996. — **138.** — P. 375-408.
11. *Johnson G. R., Beissel S. R.* Normalized smoothed functions for SPH impact computations// Intern. J. of Numerical Methods in Engineering. — 1996. — No. 39. — P. 725—2741.
12. *Swegle J. W., Attaway S. W.* On the feasibility of using smoothed particle hydrodynamics for underwater explosion calculations, Computational Mechanics. — 1995. — No. 17. — P. 151—168.
13. *Liu G. R., Liu M. B., Zong Z., Lam K. Y.* Simulation of the high explosive detonation process using SPH methodology // First MIT conference on Computational Solid and Fluid Mechanics.— June 2001, MIT, USA.
14. *Cole H.* Underwater explosions. — Princeton University Press, Princeton 1948.

Поступила 25.07.01
после доработки 30.09.02